J Mater Sci (2007) 42:4076–4086
DOI 10.1007/s10853-006-1335-6

Materials behaviour and intermetallics characteristics in the reaction between SnAgCu and Sn–Pb solder alloys

Changqing Liu · Zhiheng Huang · Paul P. Conway · Rachel C. Thomson

Received: 23 November 2005 / Accepted: 6 March 2006 / Published online: 31 January 2007
© Springer Science+Business Media, LLC 2007

Abstract The paper compares theoretical calculations with experimental data, to identify the metallurgical mechanisms with respect to the rework or repair that may be encountered in the transition period from Sn–Pb to Pb-free soldering. Thermodynamic calculations have been carried out to study material behaviour and possible formation of intermetallic precipitates during the reaction between Sn–Pb and Sn–Ag–Cu Pb-free alloys. Two Sn–Ag–Cu alloys that are relevant to current industrial interests, namely Sn–3.9Ag–0.6Cu* (known as '405 alloy' in Europe and North America), and Sn–3.0Ag–0.5Cu (known as '305' alloy in Asia), were reacted with different contamination levels of eutectic Sn–37Pb solder. The variables examined included those related to both the materials and processes, such as composition, temperature and cooling rate. Together these are the primary drivers with respect to the resultant solder microstructures, which were studied using scanning electron microscopy (SEM). Nanoindentation, which is suitable for the ultra-fine and complex microstructures, was also used to investigate the micromechanical properties, including hardness and elastic modulus, at both ambient and elevated temperatures. The results from this work provide guidance as to the consequence for microstructural evolution and hence mechanical integrity when small amounts of Pb exist in Pb-free alloys.

The composition of alloys in this paper is in weight percentage (wt%)

C. Liu (✉) · Z. Huang · P. P. Conway
Wolfson School of Mechanical and Manufacturing Engineering, Loughborough University, Loughborough LE11 3TU, UK
e-mail: C.Liu@lboro.ac.uk

R. C. Thomson
Institute of Polymer Technology and Materials Engineering, Loughborough University, Loughborough LE11 3TU, UK

Introduction

Replacing Sn–Pb with Pb-free solders has resulted in the widespread study of materials properties, processing technology and reliability for lead free solder joints in the electronic packaging community. The WEEE Directive dictates that by 1st of July 2006, Pb will be eliminated from most soldering applications in Europe. However, a number of issues related to the Pb-free soldering processes still need to be addressed. It is imperative to gain a detailed insight into the interactions of new alloys with other materials, so as to enable the optimisation and control of the processes for reliable products. A number of the developments in surface metallization to enable robust Sn–Pb soldering interconnections are now facing challenges with respect to their suitability for Pb-free alloys, which behave quite differently in their thermodynamic properties [1–5]. It is therefore important to understand the interactions and subsequent formation of intermetallic precipitates from the lead-free soldering processes. The combination of variables for Pb-free soldering is wide ranging and complicated, and depends on the specific applications, processes and materials involved, for instance there are different surface finishes to be considered (i.e. Cu, Sn, Ag, Ni–P/Au and OSP, etc.). Thermodynamic and kinetic behaviour in relation to material interactions and diffusion is an important

aspect and such knowledge can provide useful guidance in industrial applications.

In the transition period from Sn–Pb to Pb-free soldering, existing Sn–Pb products will still remain in the market or within the installed base residing with end-users of products. This will be an issue when they have to be repaired, serviced or upgraded with Pb-free solder alloys. The complete elimination of lead from the products that are specified in the legislation will have to address potential Pb contamination that is inevitable in rework or repair. A number of technical problems in connection with mixing Sn–Pb with Pb-free alloys exist:

- uncertainty of the resulting microstructure and its properties;
- the effect of unknown compositions and structures on the reliability;
- critical or tolerable levels of some elements that can be permitted in specific applications;
- the relative content of the elements and the formation and morphology of intermetallic phases.

Both experimental work [6, 7] and modelling [8–10] have been carried out to address these issues. In such circumstances, a prediction using computational methods shows its usefulness by generating the guidelines prior to practical work. The modelling allows the prediction of the possible microstructure and intermetallic phases to be formed as a function of changes in the composition of the alloys. Subsequent validation by experimental work can further confirm the theoretical results. In this work, the addition of certain amounts of Sn–Pb to Pb-free alloys are studied to provide a quantitative evaluation of the level of Pb in the alloys that could influence the formation of intermetallic phases and possibly affect solder joint performance. Different compositions were taken into account by mixing Sn–Ag–Cu alloys with eutectic Sn–Pb. Two Sn–Ag–Cu alloys: Sn–3.9Ag–0.6Cu (405), and Sn–3.0Ag–0.5Cu (305) were selected, and the Pb contamination and effects due to the mixing with eutectic Sn–Pb solder are studied both theoretically and experimentally.

In recent years, depth-sensing indentation as exemplified by nanoindentation [11] has been increasingly used to characterize the micromechanical properties of the different phases, i.e. Ag_3Sn, Cu_6Sn_5, Cu_3Sn intermetallics and the Sn matrix that are present in the lead-free solder materials [12–15]. Advanced analytical tools have also provided the opportunity to characterize the material microstructures and crystallographic features (e.g. texture) at the grain and subgrain scale. In this work, a thermodynamic modelling technique and the two aforementioned experimental methods are adopted to provide a quantitative evaluation of the different levels of Pb in Sn–Ag–Cu alloys and their influence on microstructure formation and the micromechanical properties of the alloys.

Experimental details

Thermodynamic modelling

In this study, MTDATA (version 4.73, developed by National Physical Laboratory-NPL, UK) [16] and a database containing critically assessed thermodynamic data for solder systems of 12 components (Ag–Al–Au–Bi–Cu–Ge–In–Pb–Sb–Si–Sn–Zn [17]) were employed to systematically study the microstructure of ternary Sn–Ag–Cu alloys and the corresponding quaternary system contaminated with Pb. Pb-contamination in the solder was achieved by adding the eutectic Sn–37 wt% Pb solder alloy to the Pb-free solders [6]. The compositions of the solder alloys were altered by varying the relative amount of the components (Pb-free or Sn–Pb alloys) in the system, with the Sn content always making up the balance. The total mass of the chosen system was simulated at a nominal 100 kg, unless otherwise specified. Table 1 presents the chemical compositions of the systems investigated using the thermodynamic calculations in this paper, where solder alloys 405 and 305 are represented by Sn–3.9Ag–0.6Cu and Sn–3.0Ag–0.5Cu solder alloys, respectively. Thermodynamic calculations were performed under both ''equilibrium'' (representative of slow cooling) and ''Scheil'' conditions. The Scheil calculation does not allow for any diffusion in the solid, and assumes complete diffusion in the liquid, corresponding to the worst case of segregation during cooling, and therefore is likely to be representative of non-equilibrium cooling of the solders.

Table 1 Composition of the solder alloys obtained from mixing Sn–Ag–Cu Pb-free and eutectic Sn–Pb alloys

Solders			Composition (wt%)			
Pb-free alloy	Pb-free wt%	SnPb wt%	Sn	Ag	Cu	Pb
405	95	5	Bal.	3.705	0.57	1.85
405	90	10	Bal.	3.51	0.54	3.70
405	85	15	Bal.	3.315	0.51	5.55
405	80	20	Bal.	3.12	0.48	7.40
305	95	5	Bal.	2.85	0.475	1.85
305	90	10	Bal.	2.70	0.45	3.70
305	85	15	Bal.	2.55	0.425	5.55
305	80	20	Bal.	2.40	0.40	7.40

Experimental procedure

This work has also experimentally investigated the phases present when a Sn–Ag–Cu solder alloy was melted and reacted with a eutectic Sn–Pb alloy and cooled to ambient conditions. A Sn–3.8Ag–0.7Cu solder alloy, with a composition close to the 405 alloys was reacted with a eutectic Sn–Pb alloy in a ceramic crucible (ensuring that there was no reaction between the crucible and solders). Time was allowed for the mixing and reaction between the two alloys, and then the mixture of molten solder was transferred onto a ceramic plate to effect cooling to room temperature. Finally, the microstructure and morphology of the samples were observed by optical and scanning electron microscopy (SEM), and characterized by Energy Dispersive X-ray analysis (EDX) using a Leo 1530 VP FEGSEM and an EDAX Pegasus analysis system. The samples that have been analyzed contained 5 and 20 wt% eutectic Sn–Pb solder additions, respectively. Differential Scanning Calorimetry (DSC) analyses were performed using samples of known mass, approximately ~100 mg, in a Stanton-Redcroft 1500 instrument with Orchestrator software. A correction to the absolute temperature was carried out with reference to analysis of a 99.999% pure tin sample.

Nanoindentation was carried out with a three-sided Berkovich diamond indenter mounted in a NanoTest 600 system (MicroMaterials Ltd., Wrexham, UK). The indentations were conducted using the load control mode, i.e., a loading process was completed and reversed when it reached the preset peak load. The maximum load used in this test was 2 mN, and the loading and unloading rate was set at 0.1 mN/s. Dwell times (i.e. the peak load holding period) of 20 and 60 s were applied to the tests at the room temperature (RT) and high temperature (HT), 120 °C, respectively. For the nanoindentation at HT, the indenter was pre-contacted with the sample for 5–10 min to warm up the indenter, which ensured that during the subsequent tests the indenter remained at almost the same temperature as the sample. The indentations were typically made in a 20×20 (15×15 at HT) matrix pattern. The spacing between adjacent indentations was 10 μm (15 μm at HT).

Results

Thermodynamic modelling and DSC analysis

Thermodynamic modelling is a useful tool for predicting the microstructure for a given composition of multi-component solder alloy to assist with the identification of the possible phases formed on solidification. Figure 1a, b presents the results of equilibrium calculations for the 405 alloy after the reaction with 5 and 20 wt% Sn–37Pb solders, respectively; their compositions are given in Table 1.

By adding 5 wt% Sn–37Pb to the 405 alloy, under equilibrium conditions, the liquid will begin to solidify at ~490 K (217 °C), with solidification completed within a narrow mushy range of ~15 K. The final microstructure is predicted under equilibrium conditions to consist predominantly of the β-Sn matrix with precipitates of Cu_6Sn_5 and Ag_3Sn. Pb is predicted to be soluble in the β-Sn phase at high temperature. However, once the temperature reaches about 408 K

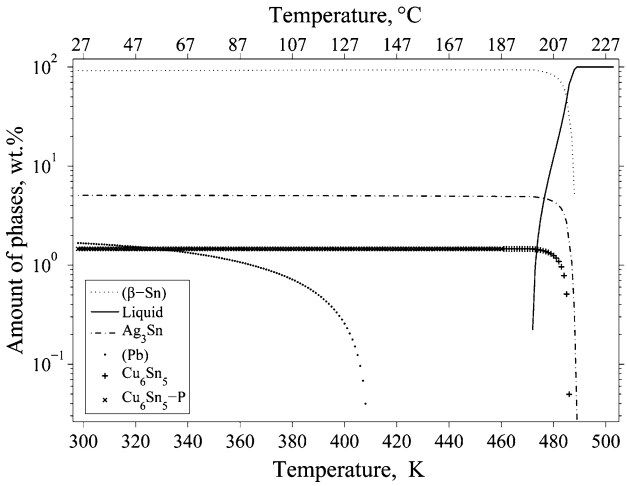

(a) *Phase formation plot for 405-5wt.%Sn-37Pb alloy*

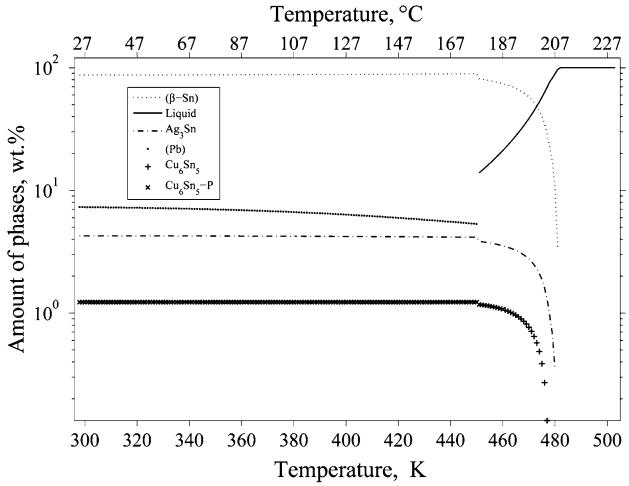

(b) *Phase formation plot for 405-20wt.%Sn-37Pb alloy*

Fig. 1 Equilibrium thermodynamic calculations for the 405 alloy with additions of the eutectic Sn–Pb solder. (**a**) Phase formation plot for 405-5 wt%Sn–37Pb alloy. (**b**) Phase formation plot for 405-20 wt%Sn–37Pb alloy

(135 °C), it can start to precipitate in the solid state to form a Pb-rich phase.

For the 405 alloy containing 20 wt% Sn–37Pb additions, the liquid starts to solidify at 480 K (207 °C), i.e. 10 K below that of the 405 + 5 wt% Sn–37Pb system. The freezing range is also widened significantly to ~30 K, and final solidification now occurs in a eutectic reaction at ~450 K (177 °C), showing close agreement with the results reported by Zeng [10]. A significant amount of a Pb-rich solid solution phase forms during the eutectic reaction from the last liquid to solidify, and will therefore be distributed in the interdendritic regions. This compares with the 405 + 5 wt% Sn–37Pb system in which precipitation of Pb was only possible in the solid state at much lower temperature.

Similar phenomena can be found for the 305 systems, which have a lower Ag content than 405 systems. Figure 2a, b presents the equilibrium calculations from the 305 alloy after reaction with 5 and 20 wt% Sn–37Pb, respectively. In comparison with 405 systems, the characteristic temperatures associated with the solidification are very similar, although the 305 alloy containing 20 wt% Sn–37Pb starts to solidify about 5° above the corresponding 405 alloy. However, the amount of intermetallic phases, Ag_3Sn and Cu_6Sn_5, varies slightly as a function of alloy content. For both 405 or 305 with 5 and 20 wt% Sn–37Pb alloy systems, thermodynamic calculations show that the transformation from the disordered Cu_6Sn_5 phase (high temperature) to the ordered Cu_6Sn_5–P phase (low temperature) occurs at ~460 K (~187 °C). Figure 3a, b illustrates the distribution of the Pb element between the phases at temperatures from 25 °C to 150 °C for the 405 + 20 wt%Sn–37Pb and the 305 + 20 wt%Sn–37Pb systems, respectively.

As shown in Figs. 1b, 2b, Pb exists as a solid solution phase below the eutectic temperature in both of these alloys, with the solubility of Pb in the Sn-rich solid solution increasing as temperature increases. It is therefore possible that thermal ageing would result in some homogenization of the Sn-rich phase. There is no solubility of Pb in either of the intermetallic phases, Ag_3Sn or Cu_6Sn_5. The presence of the low melting point Pb-rich phase is important for the reliability of such a mixture of solder joints in terms of the degradation of the mechanical integrity [10]. This is of particular importance for applications with a high service temperature (e.g. the automotive industry).

Figure 4a, b presents calculations using equilibrium and 'Scheil' models to predict the dependence of solid fraction on temperature for the 405 alloy with additions of 5 and 20 wt% Sn–37Pb, respectively. The 405

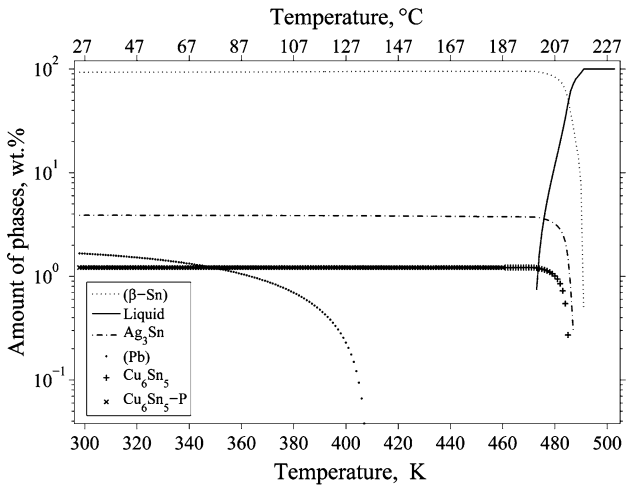

(a) *Phase formation plot for 305-5wt.%Sn-37Pb alloy (total mass of the system is assumed to be 1000 kg)*

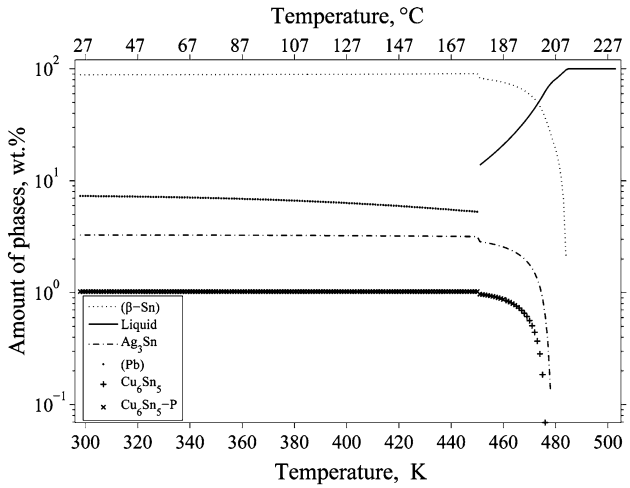

(b) *Phase formation plot for 305-20wt.%Sn-37Pb alloy*

Fig. 2 Equilibrium thermodynamic calculations for the 305 alloy with additions of the eutectic Sn–Pb solder. (**a**) Phase formation plot for 305-5 wt%Sn–37Pb alloy (total mass of the system is assumed to be 1,000 kg). (**b**) Phase formation plot for 305-20 wt%Sn–37Pb alloy

alloy without Sn–37Pb, marked as 'no contamination', was calculated under equilibrium conditions. It can be seen that the addition of Pb significantly reduces the temperature at which the last liquid can exist. Only in the case of the alloys with 5 wt% Sn–37Pb under equilibrium conditions does solidification occur above the eutectic temperature, whereas in all other cases the last liquid solidifies at the quaternary eutectic temperature of 176 °C. Therefore, a 20 K gap exists between the final solidification temperature calculated under equilibrium and Scheil conditions for the lower Pb (5 wt%) content system. This indicates that the microstructure will be sensitive to the cooling rate, which is particularly important for lower levels of Pb

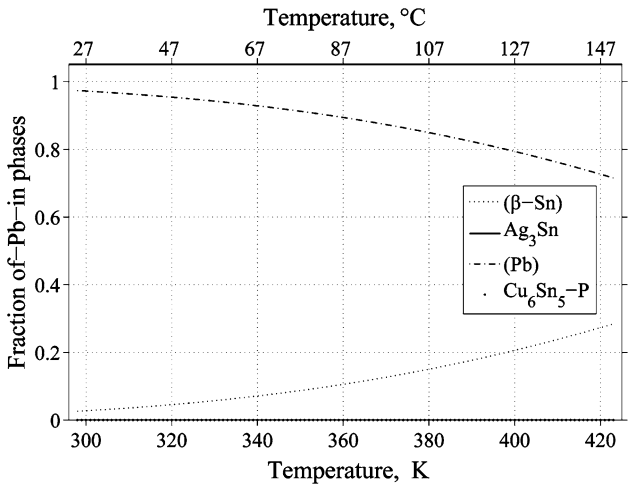

(a) *405-20wt.%Sn-37Pb alloy*

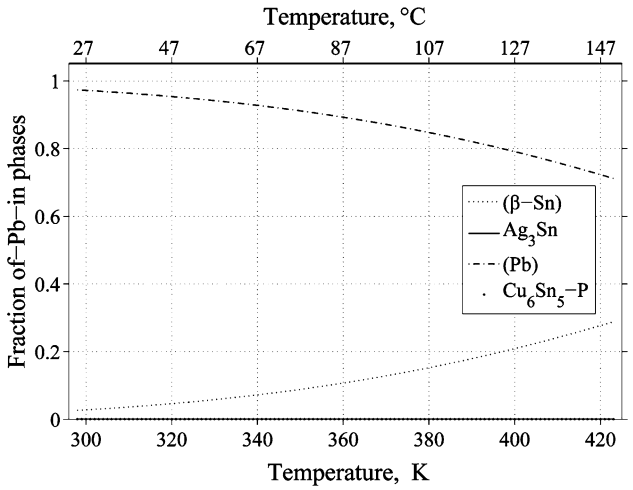

(b) *305-20wt.%Sn-37Pb alloy*

Fig. 3 Pb distributions from 25 °C to 150 °C. (**a**) 405-20 wt%Sn–37Pb alloy; (**b**) 305-20 wt%Sn–37Pb alloy

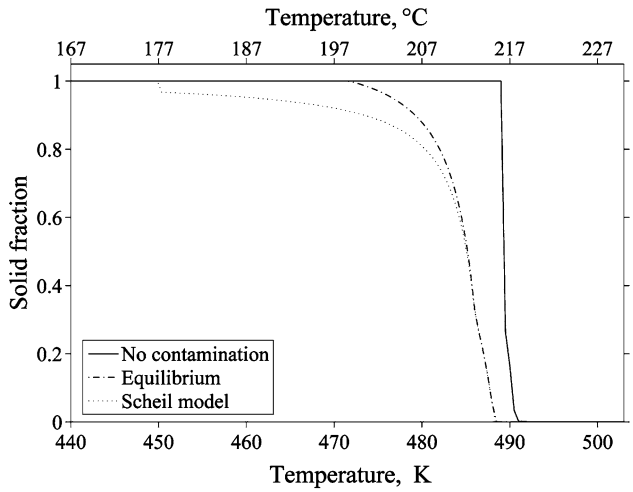

(a) *405 + 5 wt.% Sn-37Pb*

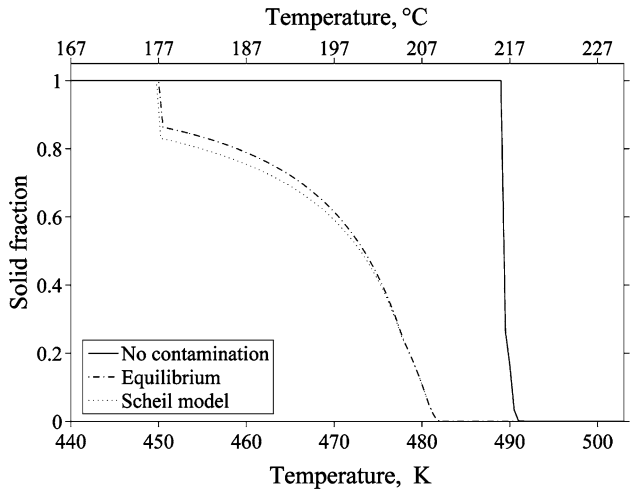

(b) *405 + 20 wt.% Sn-37Pb*

Fig. 4 Solid fractions versus temperature of 405 alloy (**a**) 405 + 5 wt% Sn–37Pb; (**b**) 405 + 20 wt% Sn–37Pb

contamination [18]. It is clear that an addition of less than 5 wt% of the Sn–37Pb solder alloy is needed to ensure that no Pb-rich phase can be present as a result of non-equilibrium segregation during faster cooling. It is also possible that the increased freezing range (or mushy range) of these systems will increase the tendency to form porosity in the final microstructure. Figure 5a, b illustrates the mass fraction of the components in the liquid phase under equilibrium and Scheil conditions. It can be clearly seen that in the lower Pb content alloy, Scheil conditions result in a steady increase in the Pb content of the liquid as partitioning occurs during solidification and therefore extends the freezing range of the alloy.

The results of the DSC analyses on the Sn–3.8Ag–0.7Cu solder alloy, and those reacted with 5 and 20 wt% eutectic Sn–Pb alloys, respectively, are presented in Fig. 6. The lower half of the graph illustrates the heating of the samples, and the top the cooling. The three alloy compositions give rise to peaks in the heat flow at different temperatures. For the two alloys containing Sn–Pb additions, the onset of melting occurs at 178 °C, which compares well with that predicted using Scheil calculations for this alloy composition, 175 °C. These two alloys can also be seen to exhibit a much larger freezing range, of the order of 40 K for the 5 wt% Sn–Pb addition and 30 K for the 10 wt% addition, compared to the Sn–3.8Ag–0.7Cu alloy. The temperature at which the sample is fully liquid decreases with increasing Sn–Pb additions.

Figure 7 illustrates the phase stability in the Sn–Ag–Cu–Pb quaternary systems by an isopleth plot created

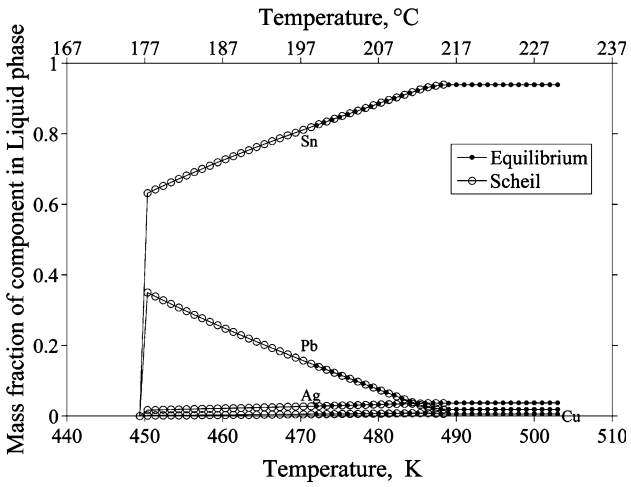

(a) *405 + 5 wt.% Sn37Pb*

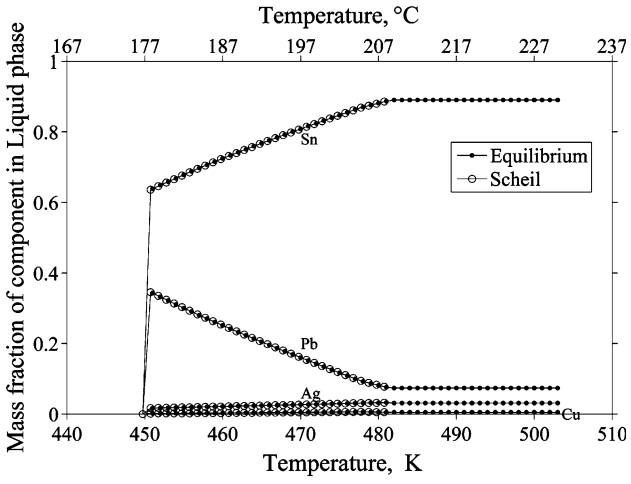

(b) *405 + 20 wt.% Sn-37Pb*

Fig. 5 The mass fraction of elements in the liquid phase under equilibrium and Scheil conditions. (**a**) 405 + 5 wt% Sn37Pb; (**b**) 405 + 20 wt% Sn–37Pb

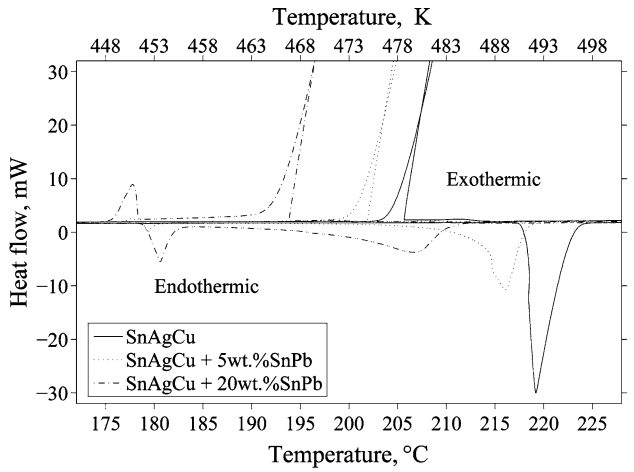

Fig. 6 DSC analyses on the Sn–3.8Ag–0.7Cu alloy, and with 5 and 10 wt% of eutectic Sn–Pb additions showing heat flow as a function of temperature

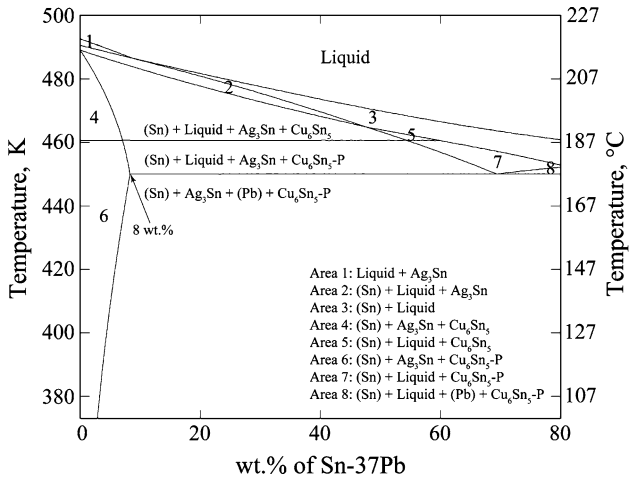

Fig. 7 Isopleth of 405 alloy with increasing Sn–37Pb

by consideration of the 405 alloy composition with increasing additions of Sn–37Pb solder. The ordering process for Cu_6Sn_5 is clearly visible, with the eutectic reaction occurring at a lower temperature than the ordering line. The diagram shows that an addition of less than ~8 wt% Sn–37Pb could be expected to avoid the formation of the Pb-rich phase through the quaternary eutectic reaction under equilibrium conditions, although as stated above, much less than this is required to guarantee its absence under more rapid cooling conditions.

Figure 8a, b shows the corresponding calculations for the 305 alloy with 5 and 20 wt% Sn–37Pb, respectively. Due to the lower Ag content, the initial solidification temperature of the 305 alloy is slightly higher than the 405 alloy, although final solidification occurs through the same quaternary reaction at ~176 °C, with no significant effect on the extent of the mushy range.

SEM observation

In order to validate the thermodynamic modelling, the microstructure of the mixture obtained from the reaction between a Sn–3.8Ag–0.7Cu solder alloy (similar in composition to 405 alloys) and Sn–37Pb was examined by SEM combined with EDX analysis. Figure 9 presents typical secondary electron micrographs showing the microstructure and distribution of intermetallics in the quaternary alloy formed from the reaction between 95 wt% Sn–3.8Ag–0.7Cu and 5 wt% Sn–37Pb solder alloys. Figure 9b highlights a pore found in this system.

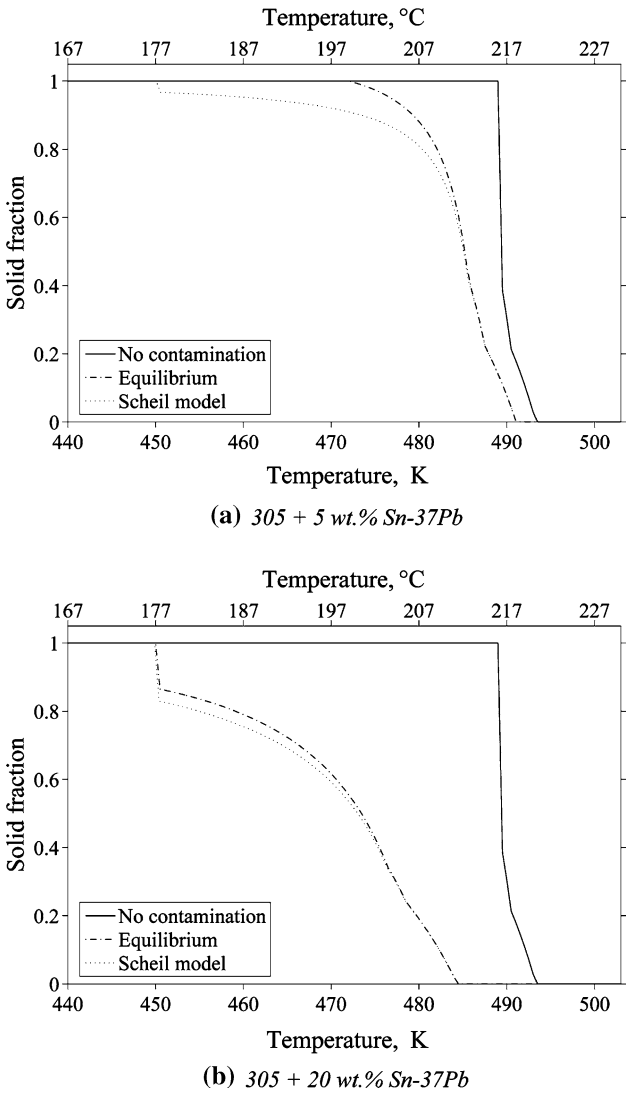

Fig. 8 Solid fractions versus temperature of 305 alloy. (**a**) 305 + 5 wt% Sn–37Pb; (**b**) 305 + 20 wt% Sn–37Pb

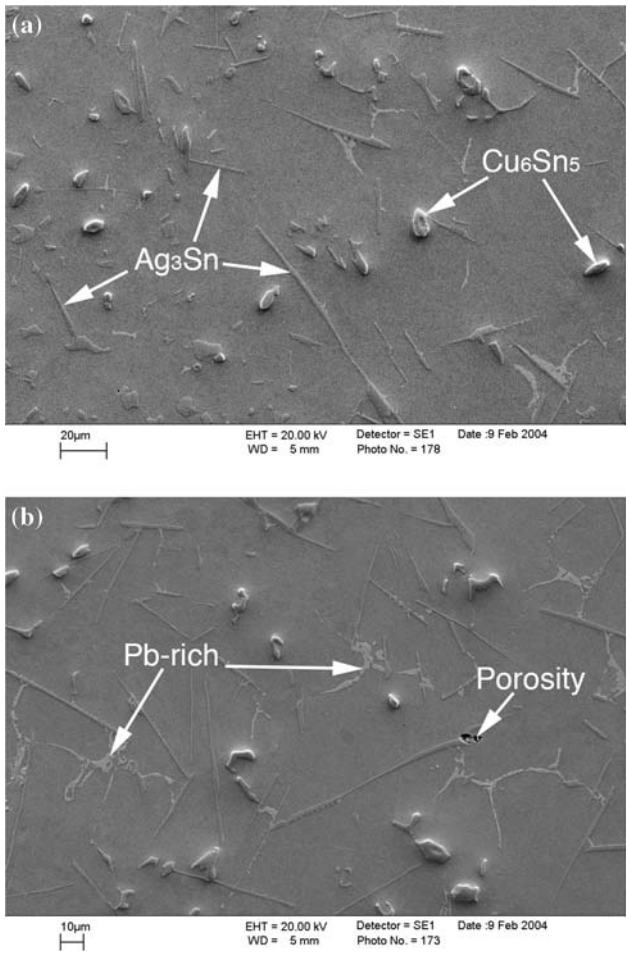

Fig. 9 SEM micrographs of microstructure and IMCs distribution of quaternary alloy formed from the reaction of 95 wt% Sn–3.8Ag–0.7Cu and 5 wt% Sn–37Pb alloys (a porosity is shown in **b**)

Cu_6Sn_5 intermetallic particles were found to be randomly distributed in the β-Sn matrix. The shape of these precipitates was irregular and blocky, exhibiting a wide range of sizes (~10–20 μm) [19]. Additionally the formation of needle-like-Ag_3Sn phases were observed, consistent with previous observations in solder joints [3–5]. Figure 9b illustrates that a Pb-rich phase precipitated discontinuously in the interdendritic regions from the last liquid to solidify during the ternary eutectic reaction as predicted. This is clearly important in respect of degradation of mechanical integrity at the high temperature.

Figure 10 presents backscattered SEM micrographs showing the microstructure of the quaternary alloy formed from the reaction between 80 wt% Sn–3.8Ag–0.7Cu and 20 wt% Sn–37Pb solder alloys. It is clear that the higher Pb content has led to a dramatic increase in the amount of the Pb-rich phase which has predominately segregated along the grain boundaries, which is observed in this case forming a virtually continuous network. Figure 10b also shows that in some cases the Pb-rich phase is visible in association with the intermetallic precipitates, which is in agreement with the results reported by Choi et al. [7] for a Sn–Ag–Pb ternary system.

Depth-sensing indentation

Hardness and elastic modulus results were obtained by mechanically probing the individual microstructural constituents using nanoindentation. Through one cycle of loading/unloading (load vs. displacement) curve, the hardness and reduced modulus value of the individual phases can be calculated [13–15]. The unloading curves of (Sn) showed that the deformation

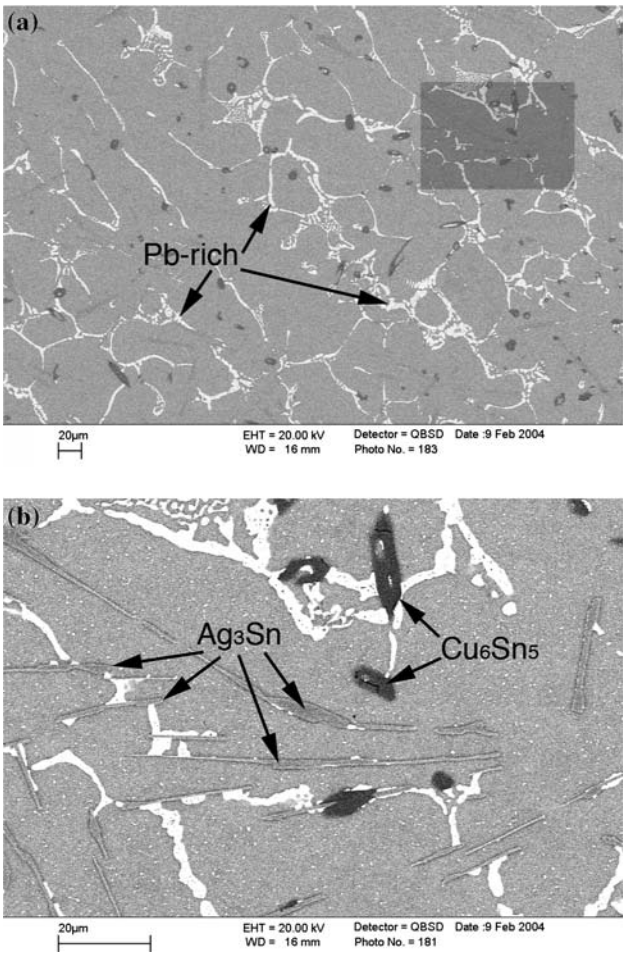

Fig. 10 SEM micrographs showing microstructure and IMCs distribution of quaternary alloy formed from reaction 80 wt% Sn–3.8Ag–0.7Cu and 20 wt% Sn–37Pb solder alloys; (**b**) is the detail of the shaded area in (**a**)

within this phase is mainly plastic [15]. However, the unloading curves of Cu_6Sn_5 and Ag_3Sn phases, however, exhibit an appreciable amount of elastic recovery after unloading. Nanoindentation can also be used to map the mechanical properties of the individual phases in particular regions of microstructure, which is useful for the correlation of microstructure and mechanical properties. Using data obtained from nanoindentation (Fig. 10a), the mechanical property mapping of a sample is constructed as shown in Fig. 10b, c. It can be seen that the mechanical property mappings match the microstructure quite well, considering the ''resolution'' for the mappings is 15 μm. However, it should be noted that the spacing of adjacent indentations should be at least 10 times the maximum width of the indentations [20] (or at least 20–30 times the maximum penetration depth [21]) to ensure that the deformed region surrounding one indentation will not interfere with the formation of the next indentation.

Discussion

The effect of Pb addition on phase formation and microstructure of Sn–Ag–Cu alloys

There have been a number of studies of the interactions between binary Pb-free solder systems (including Sn–Ag, Sn–Bi, Sn–Sb, Sn–Cu) and Sn–Pb alloys [7–10, 18]. In this work, the ternary Sn–Ag–Cu Pb-free alloys (i.e. 405 and 305) were reacted with a eutectic Sn–Pb solder, resulting in a quaternary Sn–Ag–Cu–Pb alloy. Thermodynamic calculations representing equilibrium and more rapid cooling conditions are of technological interest in the electronics manufacturing domain. The types and amount of intermetallic phases and the final microstructure is determined by the amount of the Sn–37Pb alloy added and the cooling rate. Ag_3Sn and Cu_6Sn_5 intermetallic precipitates can form in the 405 or 305 alloys, which are not affected by the addition of Pb. However, a low Pb content can lead to the precipitation of a Pb-rich phase in the solid state. A higher Pb content will result in the quaternary eutectic reaction:

Table 2 Micromechanical properties of the individual phases at RT, HT and after aging

RT	405 + 5wt% Sn–37Pb		405 + 20wt% Sn–37Pb	
	H, GPa	E_r, GPa	*H*, GPa	E_r, GPa
(Sn)	0.2 ± 0.02	40.28 ± 5.64	0.21 ± 0.03	44.52 ± 7.77
Ag_3Sn	0.89 ± 0.06	46.78 ± 5.93	1.37 ± 0.19	50.71 ± 3.23
Cu_6Sn_5	4.67 ± 0.58	88.94 ± 10.38	3.22 ± 0.57	85.58 ± 6.22
(Pb)	N/A	N/A	0.20 ± 0.02	40.90 ± 4.24
HT	405 + 5wt% Sn–37Pb		405 + 20wt% Sn–37Pb	
	H, GPa	E_r, GPa	*H*, GPa	E_r, GPa
(Sn)	0.16 ± 0.02	31.04 ± 6.50	0.18 ± 0.05	28.33 ± 5.97
Ag_3Sn	0.70 ± 0.11	25.06 ± 2.49	1.15 ± 0.0	49.34 ± 0.0
Cu_6Sn_5	2.58 ± 0.0	63.59 ± 0.0	1.20 ± 0.25	46.15 ± 5.16
(Pb)	N/A	N/A	0.09 ± 0.04	16.24 ± 1.75

$$L \rightarrow (\beta\text{ - Sn}) + (\text{Pb}) + Ag_3Sn + Cu_6Sn_5$$

resulting in the formation of a Pb-rich phase both along the cell boundaries and in association with the intermetallic phases.

The effect of Pb addition on solidification and mushy range of Sn–Ag–Cu alloys

The eutectic Sn–Ag–Cu system has a melting temperature around 490 K (~217 °C), depending on actual composition [22]. The addition of Pb results in a eutectic temperature of 450 K (~177 °C) as demonstrated in the thermodynamic calculations in this work and in agreement with literature [7, 10]. The temperature at which the liquid mixture first begins to solidify was also reduced by adding Sn–37Pb to Sn–Ag–Cu alloys; a reduction of ~3 K is predicted for a 5 wt% addition and of ~10 K for a 20 wt% addition.

It has also been shown using both thermodynamic predictions and experimental thermal analyses that Pb addition will significantly expand the freezing range of Sn–Ag–Cu solders. The mushy range of the 405 or 305 alloys can be as much as 30–40 K depending on the amount of Pb added, and the addition of Pb may limit the useful operating temperature region of the alloys.

The effect of Pb addition on the mechanical properties of Sn–Ag–Cu alloys

Table 2 presents the hardness and modulus of the constituent phases in bulk solder materials investigated. As there are no consistent Poisson ratios for all the phases involved in the present study, i.e. (Sn), Ag_3Sn, Cu_6Sn and (Pb), all the modulus data shown in Table 2 are the reduced modulus of the phases rather than a Young's modulus. The hardness and modulus values for (Sn) (usually referred to as "solder" in other studies) at room temperature are ~0.2 and ~40 GPa, respectively, which are very close to the values found in previous studies [13, 14]. No significant differences in the hardness and modulus values for (Sn) were found for the Sn–Ag–Cu solders with different levels of Pb. To date, there are apparently no micromechanical property data of the Pb-rich phase in the existing literature. It is found in this work that the Pb-rich phase has a slightly lower hardness and modulus than the (Sn) phase at room temperature. At 120 °C, a decrease in both hardness and modulus were found for (Sn) phase, however, due to its low melting point, the (Pb) phase exhibits an extremely low hardness, ~0.09 GPa, and modulus, ~16.24 GPa at 120 °C. After aging at 120 °C for 8 days, the hardness and modulus of (Sn) slightly increase whereas that of the intermetallics decreases for samples with 5 wt% addition of Sn–

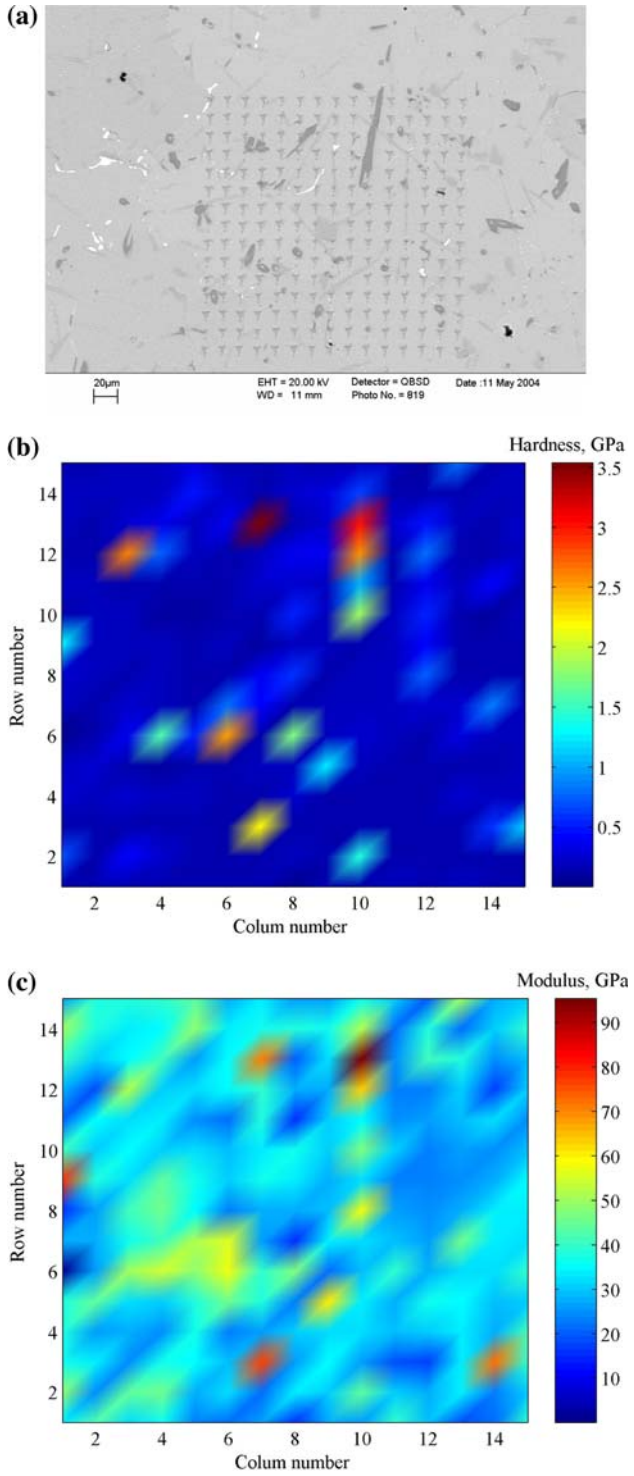

Fig. 11 Nanoindentation micromechanical properties mapping. (**a**) SEM backscattered electron image showing the indentation matrix. (**b**) Hardness mapping. (**c**) Reduced modulus mapping

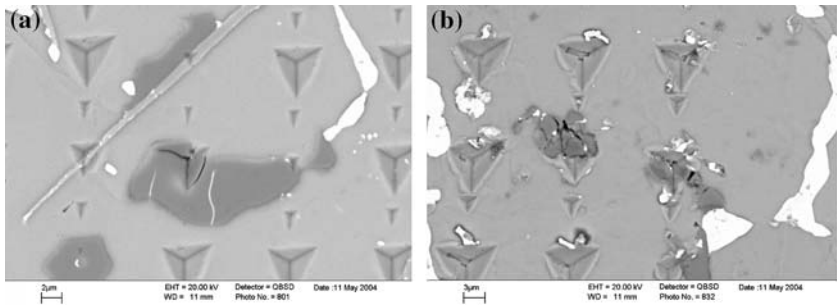

Fig. 12 Cracking of Cu_6Sn_5 phase during (**a**) RT and (**b**) HT nanoindentation test

37Pb. For the samples with 20 wt% Sn–37Pb, although (Sn) and Ag_3Sn show similar trends as in the samples with 5 wt% Sn–37Pb, the hardness of Cu_6Sn_5 apparently increased slightly. The highest hardness values for Cu_6Sn_5 and Ag_3Sn phases are 4.67 ± 0.58 and 1.37 ± 0.19 GPa, respectively. Chromik [15] found the hardness of Cu_6Sn_5 and Ag_3Sn phases, which were present in solder joints rather than bulk solder materials, to be 6.5 ± 0.3 and 2.9 ± 0.2 GPa, respectively. In addition, the indentation size effect (ISE) [14], which is exemplified by a trend of decreasing hardness with increasing indenter penetration depth, may also influence the results. Although the same maximum 2 mN load was used as in Chromik's work, penetration depths of ~100 and ~140 nm resulted for Ag_3Sn and Cu_6Sn_5 phases, respectively, whereas the corresponding penetration depths are ~130 and ~270 nm, respectively, in the present study.

Although both have higher hardness than the Sn matrix, Cu_6Sn_5 shows a much higher hardness and more brittle character than Ag_3Sn. Indeed the Cu_6Sn_5 phase was consistently observed to crack during nanoindentation in both the low and high lead containing samples. As an example, Fig. 11a shows one of the cracked Cu_6Sn_5 phases. Furthermore, the cracking of the Cu_6Sn_5 phase can also be found in the samples after nanoindentation at 120 °C (Fig. 11b). However, no evidence showing the cracking of the Ag_3Sn phase was found in this study. Therefore, more attention should be paid to the amount and morphology of the Cu_6Sn_5 phase because cracks originated in this phase could deteriorate the mechanical integrity of the solder joints (Fig. 12).

Conclusions

Thermodynamic calculations used in conjunction with a database containing critically assessed thermodynamic data for solder alloys have been used to predict the microstructural evolution for the quaternary solder systems obtained by adding Sn–37Pb to Sn–3.9Ag–0.6Cu (405), and Sn–3.0Ag–0.5Cu (305) alloys. Very good agreement is found between the predicted and experimentally observed phases present within the microstructure, and the results indicate that less than 5 wt% additions of a Sn–37Pb eutectic alloy to the Sn–Ag–Cu system is necessary to avoid the formation of the low melting point Pb-rich phase through the quaternary eutectic reaction during fast cooling, and less than ~3 wt% additions under equilibrium conditions. These results may have important implications for the use of Pb-free alloys to solder components which already contain Pb within the system.

Acknowledgements The authors wish to acknowledge financial support from the UK Engineering and Physical Sciences Research Council's (EPSRC)—Innovative Manufacturing and Construction Research Centre at Loughborough under contact No. GR/R64483/01P. The authors would like to acknowledge the support of Dr Alan Dinsdale and the National Physical Laboratory (NPL) for the provision of the MTDATA software and the solder database. The authors also wish to acknowledge Dr S. Zheng, Mr S. Birosca, Mr C.-L. Chen, Mr A. Sandaver and Mr J.S. Bates for their support in experimental work.

References

1. Bradley E (2003) Lead-free solder assembly: impact and opportunity, 53rd Electronic Components & Technology Conference, Proceedings 2003, pp 41–46
2. Zeng KJ, Vuorinen V, Kivilahti JK (2002). IEEE Trans Electron Packaging Manufact 25(3):162
3. Kang SK, Choi WK, Shih DY, Henderson DW, Gosselin T (2003) Formation of Ag_3Sn plates in Sn–Ag–Cu alloys and optimization of their alloy composition, 53rd Electronic Components & Technology, 2003, pp 64–70
4. Liu CQ, Geggel M, Conway PP (2002) Micro-scale mechanical properties of fine feature flip chip with lead free solders, 4th International Symposium on Electronic Materials and Packaging, 2002, pp 259–266
5. Liu CQ, Conway PP, Li D, Hendriksen M, Analysis of the micro-mechanical properties in aged lead-free, fine pitch flip chip joints, International Electronic Packaging Technical Conference and Exhibition, 2003, InterPACK 2003-35130
6. Zhu QN, Sheng M, Luo L (2000) Soldering Surf Mount Technol 12(3):19
7. Choi S, Bieler TR, Subramanian KN, Lucas JP (2001) Soldering Surf Mount Technol 13(2):26

8. Moon KW, Boettinger WJ, Kattner UR, Handwerker CA, Lee DJ (2001) J Electron Mater 30(1):45
9. Kattner UR, Handwerker CA (2001) Zeitschrift fur Metallkunde 92(7):740
10. Zeng XZ (2003) J Alloys Compounds 348:184
11. Oliver WC, Pharr GM (1992) J Mater Res 7(6):1564
12. Lucas JP, Gibson AW, Subramanian KN, Bieler TR (1998) Nanoindentation characterization of microphases in Sn–3.5Ag eutectic solder joints, Proc 1998 Mat. Res. Soc. Symp., San Francisco, CA, April 1998, pp 239–245
13. Chromik RR, Vinci RP, Allen SL, Notis MR (2003) JOM 55(6):66
14. Chromik RR, Vinci RP, Allen SL, Notis MR (2003) J Mater Res 18(9):2251
15. Liu C, Conway PP, Li D, Hendriksen M (2003) Trans ASME: J Electron Packaging 126(3):359
16. Davies R, Dinsdale A, Chart T, Barry T, Rand M (1989) High Temp Sci 26:251
17. Davies RH, Dinsdale AT, Gisby JA, Robinson JA, Martin SM (2002) Calphad 26(2):229
18. Huang Z, Conway PP, Liu C, Thomson RC (2003) Thermodynamic and kinetic behaviour of materials in micro joints formed with Sn–Pb and Pb-free solders. EMAP 2003, Singapore, pp 33–40
19. Hunt C, Nottay J, Brewin A, Dinsdale A (2002) Predicting microstructure of mixed solder alloy systems. NPL Report MATC(A) 83, April 2002
20. Kuhn H, Medlin D (2000) ASM handbook Volume 8: mechanical testing and evaluation (10th edn). ASM International, Materials Park, OH, pp 232–243
21. Mayo MJ, Nix WD (1988) Acta Metall 36(8):2183
22. Huang Z, Conway PP, Liu C, Thomson RC (2003) Interdependence of processing and alloy composition on the reliability of Sn-based lead free solders in fine pitch FCOB interconnection. IEMT 2003, San Jose, USA